A critical stress to detach cancer cells in microchannels

Cécile Couzon, Alain Duperray, Claude Verdier

A critical stress to detach cancer cells in microchannels

Cécile Couzon[(a)], Alain Duperray[(b),(c)], Claude Verdier[(a)]

(a) Laboratoire de Spectrométrie Physique, CNRS-Université Grenoble I (UMR 5588)
140 avenue de la physique, BP 87, 38402 Saint-Martin d'Hères cedex, France

(b) INSERM, U823, Grenoble, France

(c) Université Joseph Fourier-Grenoble I, Faculté de Médecine
Institut d'oncologie/développement Albert Bonniot et Institut Français du Sang,
UMR-S823, Grenoble, France

Abstract- We present experiments involving T24 cancer cells adhering at the bottom of functionalized microchannels, and subjected to increasing shear rates. Morphological studies have been carried out at different shear stresses. Cells exhibit spreading patterns similar to the ones observed in static conditions, as long as the shear stress is not too high. At a critical value of the wall shear stress, cells start to decrease their area until detachment is achieved for the larger stresses. The influence of microchannel size is also analyzed and shows a slight effect, enhanced for high confinement. To analyze such data, we propose a model to determine the 3D-shear stress necessary to achieve cell area decrease (leading to detachment), as a function of focal adhesion contacts present at the cell-substrate interface. Using this method, the determination of typical forces exerted at each focal contact can be achieved.

Keywords- Microfluidics, cancer cells, critical stress, focal adhesions

INTRODUCTION

The response of cells to mechanical stresses is a key factor in many biological processes like cell division, embryogenesis, cell migration, diapedesis, etc. Typical examples concern the reaction to shear stresses exerted as cells travel through the blood, or when they adhere to the vascular wall, but also within tissues, since cells are submitted to various forces due to the environment. As a first sketch, cells exert a different response as a function of substrate stiffness[15] and develop stronger forces when the substrate is more rigid[27]. They also develop larger forces as they spread[13,37] or as the ligand concentration increases. Cells might also change their orientation as a function of environmental anisotropy, leading to cell polarization as shown in recent experiments on specific micropatterned surfaces[41]. But their orientation might also depend on the type of forces to which they are subjected to, like static, quasistatic or periodic stresses[13]. Reaction to mechanical stresses involves mechanotransduction, the reorganization of the cytoskeleton, as well as the formation or disruption of focal adhesions. For example focal contacts can act as mechanosensors and enable growth of further adhesion sites[38] in the case of adhering fibroblasts. An additional effect is the actin reorganization of a cell under flow, as shown for example with Dyctiostelium discoideum[12]. Flow reversal leads to a change in cell polarity, corresponding to relocalization of an actin-rich region opposite of the flow. In other words, cells are able to modify their local rheological properties[43] in order to achieve a particular response.

Many experiments have been achieved in the past for studying cell behaviour under flow, as a particular way to apply mechanical stresses to adhering cells. This aspect is particularly important when trying to model leukocyte/cancer cell interactions with the endothelium[44]. Indeed, circulating cells first interact with the endothelium and cells activate to form weak bonds leading to cell rolling[25], followed by mechanotransduction and the formation of stronger bonds, allowing cells to adhere, spread and eventually transmigrate across the endothelial monolayer. During this process, it is important to determine what forces are necessary to detach such bonds (i.e. when tumor cells adhere to the endothelium), and to determine whether cells are able to resist against the flow[10]. Another important application is the transport of cells in microchannels which is now becoming very promising, especially with the recent advances of microfluidics which could allow the sorting of normal cells vs. cancer cells. Experiments on the influence of a controlled flow rate (or

shear stress) on adhering cells have been performed in parallel plate flow chambers[6,9,35] or radial flow experiments[14], or with micropipettes[4,11,31]. Such devices allow to control the applied shear stresses, usually chosen in the range [0.1-2 Pa] as in physiological conditions. Particular attention has been given to endothelial cells under flow conditions. Thoumine et al.[42] showed that endothelial cells become elongated in the flow direction in an almost regular manner, and that the underlying actin cytoskeleton also seems to align in the same direction. Chachisvilis et al.[7] finally demonstrated the role of G-protein coupled receptors, which act as mechanosensors.

To further investigate the response of a cell exposed to a flow field, it is necessary to find out theoretically which forces and torques are applied to the adhering cell, depending on flow geometry. Pozrikidis[36] determined numerically forces and torques exerted by a 3D shear flow on an adhering cell, assuming the cell to be a spherical cap or an ellipsoid, but the study was limited to an infinite flow domain. Gaver and Kute[19] studied analytically and numerically the effect of flow on a 2D adherent cell in a microchannel and generalized this idea to the 3D-case, coming up with simple formulas depending on confinement. Once the flow field is known, models of adhesion and detachment can then allow to determine dissociation rate constants[21], since cell detachment is controlled by the ability of cells to form bonds between its receptors and the corresponding ligands on the surface. Still it is not known what are the precise mechanisms by which cells spread and adhere under flow.

Therefore the purpose of the present study is to focus on experimental results where cells adhering to the walls of a microchannel are subjected to an increasing shear flow until detachment. This implies modifications of the cells morphology, in relation with their adhesion properties and the flow characteristics. This is not only relevant for microfluidics, but is also a true situation encountered in post capillary venules ($5 - 200\,\mu m$ in size) where circulating cells interact with the vessel walls and adhere. Recent developments have enabled the study of cell migration[8,23,39] and adhesion strength[20,24,28,45] in confined geometries. Most of these studies consist in end-point assays, i.e. measuring the total distance the cells migrate or counting the fraction of remaining adherent cells at the end of the experiment. The present motivation is here to analyze carefully the cell behaviour, in particular what exact stresses or forces are necessary to achieve cell detachment, and how this can be related to cell adhesion. We will focus on a particular type of cancer cells (T24, an epithelial bladder type) and investigate the action of a flow field while comparing it with the adhesion sites

formed below the cell. This study can serve as an interesting tool for estimating the typical force per adhesion site by which this type of cell adheres to a given substrate. This can be obtained thanks to fluorescence microscopy observations of focal adhesions, enabling the count of such adhesion sites and their size.

The paper is organized as follows. In the first part, we describe materials and methods, in particular cells, microchannels build–up, fluorescence microscopy, and the working equations governing flow parameters. Then results are collected to describe cell spreading and detachment, in order to propose a new method for determining the critical stress for cell retraction. In the final part, the effect of confinement on the critical shear stress is discussed, then we use a model based on previous work[19] to interpret our data and come up with the missing parameters in the adhesion model. This enables us to determine typical forces involved at each focal adhesion site. Such results obtained for this type of cells are then compared with previous studies.

MATERIALS AND METHODS

Cell culture

T24 is a human epithelial bladder cancer cell line. In our experiments, T24 cells were cultured in $25\,\mathrm{cm}^2$ tissue culture flasks (T25) at 37° C, in a humidified atmosphere with 5% CO_2. The cells were incubated in RPMI supplemented with $100U/mL$ penicillin and $100\mu g/mL$ streptomycin and 10% fetal calf serum. Cells were grown to near confluence in the culture flasks and then suspended with 0.05% trypsin-EDTA solution. The concentration of suspended cells was determined using a Neubauer cell, before being introduced into the microfluidic chip.

Long term experiments under static conditions

T24 cells in culture medium were placed on a glass slide recovered by a thin layer of PDMS ($< 0.5mm$). Cells were left to sediment and spread in static conditions. Phase-contrast images were taken every five minutes. The substrate and the coating were the same as in microchannels, consequently these experiments under static conditions can be used as a control for the experiments under flow conditions.

Design of microfluidic devices

The microfluidic devices were made using the PDMS rapid photolithographic technique according to previous works[17]. The photolithography masks bearing the channel design were printed on high resolution films. The negative masters were then created from a photo–patternable epoxy (SU-8, Gersteltec) spin-coated onto silicon wafers, and exposed to UV light through the film negative of the desired channel size. The silicon was then etched with inverse structures of the microfluidic channels : typically $1\,mm$ width (w) and $50-300\,\mu m$ height (h). The PDMS elastomer devices were molded from the masters using two-part Sylgard silicon elastomer (a mixture of 1:10 silicon elastomer and curing agent degased and poured against the silicon master). Once cured, each PDMS device was punched with inlet/outlet holes, treated with air plasma (2.10^{-4} bar at $6.8W$ coil power for 40 seconds), bonded to the glass slide by putting both treated surfaces in contact to each other immediately after, and connected to tubes which were sealed with glue (Araldite). In order to prevent bubbles from entering the channel, a bubble trap was also included into the microfluidic device as shown in Fig. 1.

Channel coating and cell loading for shearing experiments

Prior to each experiment, the microchannel walls were functionalized with a fibronectin solution ($20\mu g/mL$) for one hour at a typical flow rate of $0.8mL/h$ in order to allow fibronectin adsorption onto the treated PDMS surfaces. The bubble trap was then filled with culture medium. Finally the channel was rinsed for 15 minutes with culture medium.

Cells in suspension at a concentration adapted to the channel size (in the range $1-5.0\,10^6$ cells/mL) were pumped into a microfluidic device at a small flow rate Q corresponding to a small wall shear stress (in the connection tube) less than $0.1Pa$. Typically $Q = 10\,mL/h$ in a cylinder of radius $r = 0.4mm$, $\eta \sim 10^{-3}Pa.s$ at 37° C, which leads to a wall shear stress in the connection tube $\sigma = 4\eta Q/\pi r^3 = 0.055Pa$. Once located in the channel, cells were left at rest for 15 minutes to allow attachment to the channel wall.

Experiments under controlled flow conditions

Shearing experiments were performed to investigate cells responses and their ability to resist the flow. In particular, measurement of the cell area over a range of shear stresses

is important to determine the effect of flow on adherent cells. During measurements, a continuous flow was applied and a region of interest (ROI) in the center of the channel was investigated at fixed time intervals (15 seconds). The flow rate was changed regularly every 5 minutes, starting at low flow rates and then increasing, inducing higher shear stresses progressively. In all cases, the Reynolds number given by $Re = \rho V D_h/\eta$ was less than 130 (where $D_h = wh/2(w+h)$ is the hydraulic diameter and V the mean fluid velocity), indicating that the flow was laminar. Images were taken at the center of the channel, away from the side walls, to ensure the full development of the velocity profile. Individual cell morphologies (area, angle, aspect ratio, etc.) were recorded in real time using phase contrast microscopy. A global view of the experimental set-up can be seen in Fig. 1.

Figure 1.

Determination of the Wall Shear Stress

To determine the Wall Shear Stress (WSS), the stress vector on an oriented facet (normal unit vector $\overrightarrow{n}$) is introduced: $\overrightarrow{t}(\overrightarrow{n}) = \mathbf{\Sigma}.\overrightarrow{n}$. $\mathbf{\Sigma}$ is the shear stress tensor, given by $\mathbf{\Sigma} = -p\mathbf{I}+2\eta\mathbf{D}$ for a Newtonian incompressible fluid, η is the fluid viscosity, $\mathbf{D}$ is the symmetrical part of the fluid velocity gradient tensor and p is the pressure. $\overrightarrow{v}$ is the fluid velocity and only has a $z-$component depending on x and y, in the coordinate system shown in Fig. 2 because of the translational invariance.

Consequently the shear stress depends on the velocity field $\overrightarrow{v}$ which is described by the Stokes equation. In the case of an incompressible Newtonian fluid, the fluid velocity $\overrightarrow{v}$ and the pressure p are solutions of the system:

$$\begin{cases} \operatorname{div}\overrightarrow{v} & = 0 \\ -\overrightarrow{\operatorname{grad}}p + \eta\Delta\overrightarrow{v} & = 0 \end{cases} \tag{1}$$

together with boundary conditions $\overrightarrow{v}(-\frac{w}{2}, y, z) = \overrightarrow{v}(\frac{w}{2}, y, z) = \overrightarrow{v}(x, 0, z) = \overrightarrow{v}(x, h, z) = \overrightarrow{0}$, where ρ is the fluid density.

Figure 2.

The previous system (1) can be solved using Fourier series decomposition[46]. Assuming a constant pressure gradient $\Delta p/L$ (where Δp is the pressure drop over the length of the channel L) corresponding to the channel sketched in Fig. 2, the solution reads :

$$v_z(x,y) \;=\; \frac{\Delta p}{\eta L}\frac{4h^2}{\pi^3}\sum_{n=1,3...}^{\infty}\frac{1}{n^3}\left(1-\frac{cosh(\frac{n\pi x}{h})}{cosh(\frac{n\pi w}{2h})}\right)\sin\left(\frac{n\pi y}{h}\right) \tag{2}$$

with $-w/2 < x < w/2$ and $0 < y < h$.

This allows to determine the component of the stress tensor $\mathbf{\Sigma}$ of interest, i.e. $\sigma_{zy} = \eta\frac{\partial v_z}{\partial y}$, related to the wall shear stress at $y = 0$ in the absence of cells :

$$\sigma_{zy}=\frac{\eta Q\pi^2}{2h^2}\frac{\sum_{n=1,3...}^{\infty}\left[\frac{1}{n^2}\left(1-\frac{cosh(\frac{n\pi x}{h})}{cosh(\frac{n\pi w}{2h})}\right)cos\left(\frac{n\pi y}{h}\right)\right]}{\sum_{n=1,3,5...}^{\infty}\frac{1}{n^4}\left[w-\frac{2h}{n\pi}\tanh\left(\frac{wn\pi}{2h}\right)\right]} \tag{3}$$

Q is flow rate, w and h are respectively the channel width and height. σ_{zy} is the stress felt by the cell if it were flat, since it corresponds to the main shear forces exerted by the fluid. We will see in the final section that this value can be affected by the presence of a cell. To determine the evolution of the shear stress in the microchannel, calculations were made using the *Scilab* software.

Figure 3.

For a thin channel ($w \gg h$), the equation (3) can be simplified and the WSS has an almost constant value across the channel x–axis (except in a narrow region close to the vertical edges) given by equation (4) and also shown in Fig. 3.

$$\sigma_{zy} \sim \frac{6\eta Q}{wh^2} \tag{4}$$

This is usually a good assumption in our experiments, with w of the order of $1\,mm$ and h ranging between 50 and $250\,\mu m$.

Data analysis

Measurements were done on time-lapse images of the cells by drawing contours using a graphical pad (see Fig. 4). Area, perimeter, circularity and ellipse parameters (axes, angle) were obtained using the ImageJ software (NIH Image, Bethesda, USA). The cell area $A(t)$ was plotted versus time as shown for instance in Fig. 5a (flow rate increased every 5 minutes). $A(t)$ was fitted by a polynomial and the mean slope was calculated from this polynomial fit for each flow rate corresponding to a determined WSS. Thus the slope $\frac{dA}{dt}$ (corresponding to the area change) was plotted versus the WSS for each value of the applied flow rate or WSS giving rise to discrete data (Fig. 5b). Since the applied duration of each flow rate was short, this allowed to obtain sufficient data for determining the critical value of the WSS (i.e. WSS_c), this value being the WSS that gives a zero–slope, therefore a maximum in cell area.

Figure 4.

Figure 5.

Immunofluorescence

After application of the stress cycle, right on the plateau (after $3\,Pa$), cells were fixed using PBS containing 3% of Paraformaldehyde (PFA) for $10\,min$. Membranes were permeabilized with PBS containing 1% Triton X100 for $10\,min$. Then the system was rinced with PBS. A first wash was made with a solution of PBS containing 0.2% Saponine and 2% BSA. A first antibody was used (human antipaxillin) for $30\,min$, followed by a second wash (same as before). The second antibody TRITC (Tetramethyl Rhodamine Iso Thio Cyanate) was then used for $30\,min$ under darkness conditions, followed by a third wash. The channel was then filled with a DAKO mounting medium. Microscopic observations were made using combined phase contrast and fluorescence.

RESULTS

In order to understand how cells behave under flow conditions, we first need to have a reference which is the spreading behaviour with no applied flow. This will allow to determine relevant cell shapes and typical times. Under static conditions, cells sediment, then they spread on the substrate (spreading does not occur at the same time for all cells). In most cases, spreading is fast and the maximum area is reached in less than 45 minutes as shown in Fig. 6a. After this spreading step, eventually followed by random migration on the substrate, some cells retract their protrusions (corresponding to the area decrease in Fig. 6a) to reach a round shape and divide into two daughter cells.

Figure 6.

To take into account only viable cells, we decided to observe only daughter cells. Actually, a cell divides only when under good culture conditions, and cell division gives two healthy daughter cells. During the experiment in static conditions, eleven divisions were recorded, which means twenty–two daughter cells. For each division, the contour of the daughter cells was drawn and the cell areas were measured one hour after division. To decide which areas are to be selected, we determined the statistics of our population of daughter cells. The distribution of viable cells area is given in Fig. 7. Cell areas were in the range $800-1600\ \mu m^2$, with a maximum in the range $1000-1100\ \mu m^2$. The mean area is $1118 \pm 248\ \mu m^2$. This is the range that we selected in our experiments.

Figure 7.

T24 cells adherent at the bottom of microchannels were submitted to increasing shear flows. We observed a biphasic behaviour: cell area first increases at low WSS, then decreases for higher values of the WSS. Typical phase–contrast images are shown in Fig. 8. The cell first adheres and spreads along the channel wall as in Fig. 8(a)-(b), while keeping a round shape with a prominent nucleus and a large lamellipodium around it. As the flow rate is increased (i.e. WSS increases), the cell area starts to decrease (Figs 8(c)-(d)) until the cell

eventually looses its adherence as shown in Fig. 8(e) just before detachment.

Figure 8.

To analyze this data further, the time evolution of the area $A(t)$ of five cells is presented. Area versus time plots confirm that cell areas first increase at low WSS values (WSS values less than 3 Pa), as it can be seen in Fig. 9 which illustrates the behaviour of five cells under the same flow conditions. When the WSS is increased further, cell area increases slowly until the area reaches a maximum (as shown by the stars in Fig. 9). When the WSS increases further, the area decreases with time. The maximum area corresponds to a zero–slope for $\frac{dA}{dt}$ i.e. the transition between positive and negative values of the area rate of change $\frac{dA}{dt}$ (as shown for example in Fig. 10 where the slope is plotted against the applied WSS). From the polynomial fit and its derivative, we determine the slopes $\frac{dA}{dt}$. We assume a constant slope for each $5\,min$ time interval during which a constant WSS is applied ($0.1 - 29.6\ Pa$) as in the example shown in Fig. 10. The slope cuts the zero axis at a critical value of the WSS (WSS $_c$) corresponding to the maximum area (arrows in Fig. 10). Typical values of WSS_c are between 1 and 5 Pa, as shown in Fig. 11.

Figure 9.

Figure 10.

To investigate the influence of the confinement, experiments were carried out (at least five cells) to measure Mean $\pm$ SD of the WSS_c in channels with three different heights in the range $60 - 260\ \mu m$. We found that WSS_c slowly increases when channel height increases as shown in Fig. 11. We note that for very small heights h, the critical stress for the onset of detachment becomes smaller, since larger stresses are involved in confined channels.

Figure 11.

DISCUSSION

We need to correlate the WSS to the adhesion resistance, i.e. the forces generated by cells adhering at the wall to resist the flow. In confined geometries, the fluid is constrained by the channel walls, which leads to an increase in the flow resistance when an object partially blocks the channel. Consequently, the shear stress (WSS) really felt by adherent cells in the microchannel is roughly three times higher than the shear stress at the bottom of a cell–free channel[19]. The same studies have shown that for a semi-circular bulge attached to a microchannel wall in a confined vessel, the force $\overrightarrow{F_{flow}}$ and the torque value $\overrightarrow{T_{flow}}$ (around the axis going through the center of mass) induced by the flow can be generalized from 2D–simulations to the 3D–case. Explicit formulas for such force and torque are given by:

$$\overrightarrow{F_{flow}} = 24\eta\gamma^2 \frac{Q}{w} \frac{3.19 + 0.65\gamma + 4.34\gamma^2}{(1-\gamma^2)^{5/2}} \overrightarrow{e_z} \tag{5}$$

$$\overrightarrow{T_{flow}} = 12\pi\eta\gamma^2 \frac{RQ}{w} \frac{1.15 + 0.7\gamma}{(1-\gamma^2)^{5/2}} \overrightarrow{e_x} \tag{6}$$

where η is the fluid viscosity, R the cell radius, Q the flow rate, and $\gamma = \frac{R}{h}$ is the degree of confinement (h being the channel height).

Figure 12.

In this case, due to the fact that the channel width is larger and according to the WSS calculation (see § *WSS calculation*), we can assume that this result is quite relevant.

Since the cell area decreases above a certain typical hydrodynamic force, we conclude that, above this typical value of the hydrodynamic stress, bonds are more likely to break than to form, leading to a decrease in total adhesive force. Thus there exists an equilibrium between the effect of hydrodynamic forces and adhesive forces, corresponding to the critical stress that was determined by this method. The hydrodynamic force is given in equation (5).

Let us try to determine the force due to adhesive resistance of the cell that counterbalances the hydrodynamic force. We consider a cell as a half-sphere of radius R, and assume a distribution of N adhesion sites on the whole cell-substrate contact area S, which is supposed to be circular (radius R_t). An estimation of R_t was obtained in the experiments $R_t \sim 26 \pm 2\ \mu m$, as will be justified later. A force $\overrightarrow{f_{ad}}$ (which can be decomposed into a vertical component $f_{ad_y}\overrightarrow{e_y}$ and an horizontal component $f_{ad_z}\overrightarrow{e_z}$) is applied at each focal adhesion site (see Fig. 12). The total adhesion force $\overrightarrow{F_{ad}}$ is the sum of the individual forces $\overrightarrow{f_{ad}}$: $\overrightarrow{F_{ad}} = \sum \overrightarrow{f_{ad}}$, and its components can be determined by summing the components of individual adhesion forces as done in the system (7):

$$\begin{cases} F_{ad_z} = \sum f_{ad_z} = N f_{ad_z} \\ F_{ad_y} = \sum f_{ad_y} = N f_{ad_y} \end{cases} \tag{7}$$

When in equilibrium, adhesion forces counterbalance hydrodynamic effects and the cell does not spread any longer but still holds onto the substrate, therefore the hydrodynamic force $\overrightarrow{F_{flow}}$, which is along the z axis ($\overrightarrow{F_{flow}} = F_{flow}\overrightarrow{e_z}$), is balanced by the horizontal component of the adhesion force F_{ad_z}:

$$F_{flow} = F_{ad_z} \tag{8}$$

In the hydrodynamic force estimation[19], the cell is represented by a semi-circular bulge of radius R and F_{flow} reads:

$$F_{flow} = 24\eta\gamma^2 \frac{Q}{w} \frac{3.19 + 0.65\frac{R}{h} + 4.34\left(\frac{R}{h}\right)^2}{(1 - \left(\frac{R}{h}\right)^2)^{5/2}} \tag{9}$$

Using equation (8)–(9), we obtain:

$$24\eta \left(\frac{R}{h}\right)^2 \frac{Q}{w} \frac{3.19 + 0.65\frac{R}{h} + 4.34\left(\frac{R}{h}\right)^2}{\left(1 - \left(\frac{R}{h}\right)^2\right)^{5/2}} = N f_{ad_z} \tag{10}$$

where WSS can be introduced using its value $6\eta Q/wh^2$ from equation (4). So the critical value of the WSS becomes:

$$WSS_c = N f_{ad_z} \frac{1}{4R^2} \frac{\left(1 - \left(\frac{R}{h}\right)^2\right)^{5/2}}{3.19 + 0.65\frac{R}{h} + 4.34\left(\frac{R}{h}\right)^2} \tag{11}$$

The values of WSS_c versus h are calculated for three values of the adhesion parameter $Nf_{ad_z} = 10\ nN$, $30\ nN$ and $50\ nN$ using $R = 18\ \mu m$. Results are shown in Fig. 13.

Figure 13.

For small channels ($h < 100\ \mu m$), the WSS increases rapidly with channel height h. The increase for higher channels is much slower and shows a plateau when h becomes large: $\lim_{h\to\propto} WSS_c = \frac{Nf_{ad_z}}{12.76R^2}$. This is in agreement with our experimental data: for the three channel sizes used in the experiments, WSS_c increases with h. Fitting of the experimental data with the results of the model (11) has been carried out using Nf_{ad_z} as a parameter (see Fig. 11). Results of the fit give a good correlation (using $R = 18\,\mu m$ as a good estimation of the cell height), corresponding to an approximate horizontal component of the adhesion force $F_{ad_z} = Nf_{ad_z} = 18\ nN$.

Thus our modeling approach leads to the total adhesion force component in the plane corresponding to the cell-substrate contact $F_{ad_z} = 18\ nN$. Although cell adhesion properties are cell and matrix–dependent[47], estimates of the forces involved can be discussed. Different techniques have been elaborated to determine cell traction forces exerted by cells on a given substrate. For example, the displacement of fluorescent beads embedded in a soft polyacrylamide gel onto which cells adhere allow to determine the traction field, i.e. the local force per unit area (or per unit adhesion site) imposed by the cell. Maximum traction forces for T24 cells, HASM cells, and 3T3 fibroblasts spread on polyacrylamide gels (elasticity modulus around $2kPa$) have been found to be respectively $0.05\,kPa$[1], $0.4\,kPa$[5] and $2\,kPa$[32]. As it can be seen on fluorescent images[2,3,34], focal adhesion sizes are usually in the range $[1-5\mu m^2]$. These observations lead to traction forces between $0.05\ nN$ and $10\ nN$ per focal adhesion site.

Other studies using cells adhering to flexible micropillars give access to the same traction forces, correlated to focal adhesion sites located on the top of such micropillars. Fibroblasts and smooth muscle cells grown on such PDMS microposts develop cellular traction forces comprised between $1\ nN$ and $10\ nN$[2,26], whereas for individual epithelial cells migrating on micropillars[18], maximal forces reached $3\ nN$. Altough the present situation is not that of a migrating cell, it can be useful to compare the data given above to our case, since it is

important to find out how much traction a cell can exert on a substrate.

In order to be more accurate, we carried out immunofluorescence experiments after fixing the T24–cells, following the application of the previous stress cycle. Then cells were stained for immunofluorescence recognition of the paxillin molecule involved in the focal adhesion complexes. This is shown in Fig. 14, where three images are provided after application of stresses until the area plateau is reached. The first image is a phase contrast one for identification of cell contours thus providing the area, whereas the second one shows the location of paxillin, which appears mainly at the cell edges through several focal contacts. Finally we used image processing to determine the number of adhesion zones (third image), their average area and their total size. This leads to the identification of 31 such zones, with an average area of $2.5\,\mu m^2$, for a total area of $78\,\mu m^2$. Meanwhile, the cell area is around $2140\,\mu m^2$, corresponding to a radius $R_t = 26\,\mu m$. Note that the number of focal adhesions (31) is in agreement with previous *in vivo* observations of leukocytes adhering to the endothelium[22] giving rise to about 30 sites, or to a similar number (around 50) in the case of adhering rat embryonic fibroblast cells[34].

Figure 14.

Therefore, based on the number of focal adhesions and their size (as determined from Fig. 14), we can estimate the average force per focal site to be about 0.58 nN, or an equivalent stress of about $230 Pa$ at each focal adhesion site. This is in the range of the maximum stresses found for migrating T24–cells[1] on a $10\,kPa$–substrate, where a maximum value of $200\,Pa$ was found for the traction stress. In the present case, the PDMS Young's modulus used for the microchannel is roughly $0.6\,MPa$. Therefore, the present results seem to be quite realistic. Finally, let us note that the forces exerted by such cancer cells are rather small, as compared to fibroblasts[2].

CONCLUSIONS

A microfluidics experiment has been carried out to detach cancer cells adhering to the bottom of a micro–fabricated channel. The analysis of the cell morphology has revealed the cell resistance to increasing flow, until a critical stress WSS_c is reached. This critical stress is a function of the product $N\, f_{ad_z}$ of adhesion sites number N with their strength f_{ad_z}, as well as the ratio h/R, h being the channel height and R the cell height. When h/R decreases, the sensitivity of WSS_c to h/R becomes more pronounced, whereas it reaches a constant limit at large h/R. This rather simple experiment was combined with fluorescent assays to allow the determination of the forces developped at each focal site. Although this analysis contains estimates, it seems to be able to predict adhesion parameters rather well, when compared to previous studies related to traction forces exerted by adhering/migrating cells. It also confirms a previous result showing that such cancer cells exert small forces, therefore they can move faster. Further fluorescence studies are now needed to correlate more precisely the distribution of adhesion sites (size, number, position) as a function of the applied shear stress.

ACKNOWLEDGMENTS

The authors thank the European Commission Marie Curie Research Training Network MRTN-CT-2004-503661 "Modelling, mathematical methods and computer simulation of tumour growth and therapy" (http://calvino.polito.it/ mcrtn/) for its support. We are also thankful to V. M. Laurent for helpful discussions and reading of the manuscript.

REFERENCES

[1] Ambrosi, D., A. Duperray, V. Peschetola, C. Verdier. Traction patterns of tumor cells. *J. Math. Biol.* in press, doi 10.1007/s00285-008-0167-1, 2008.

[2] Balaban, N. Q., U. S. Schwarz, D. Riveline, P. Goichberg, G. Tzur, I. Sabanay, D. Mahalu, S. Safran, A. Bershadsky, L. Addadi and B. Geiger. Force and focal adhesion assembly: a close

relationship studied using elastic micro-patterned substrates. *Nat. Cell Biol.* 3:466–472, 2001.

[3] Bershadsky, A. D., N. Q. Balaban and B. Geiger. Adhesion-dependent cell mechanosensitivity. *Annu. Rev. Cell Dev. Biol.* 19:677–695, 2003.

[4] Bohnet, S., R. Ananthakrishnan, A. Mogilner, J-J. Meister and A. B. Verkhovsky. Weak force stalls protrusion at the leading edge of the lamellipodium. *Biophys. J.* 90:1810–1820, 2006.

[5] Butler, J. P., I. M. Tollic-Norrelykke, B. Fabry and J. Fredberg. Traction fields, moments, and strain energy that cells exert on their surroundings. *Am. J. Physiol.* 282:C595–C1605, 2002.

[6] Cao, J., B. Donell, D. R. Deaver, M. B. Lawrence and C. Dong. In vitro side-view imaging technique and analysis of human T-leukemic cell adhesion to ICAM-1 in shear flow. *Microvasc. Res.* 55:124–137, 1998.

[7] Chachisvilis, M., Y-L. Zhang and J. A. Frangos. G-protein coupled receptors sense fluid shear stress in endothelial cells. *Proc. Natl. Acad. Sci. USA* 103:15463–15468, 2006.

[8] Chaw, K. C., M. Manimaran, E. H. Tay and S. Swaminathan. Multi-step microfluidic device for studying cancer metastasis. *Lab Chip* 7:1047–1047, 2007.

[9] Chotard-Ghodsnia, R., A. Drochon, N. Faucheux, M. D. Nagel and R. Grebe. Effect of shear stress and of transmural pressure on cAMP-dependent responses of cells adhering to a biomaterial. *Eur. Phys. J. AP* 17:155–162, 2002.

[10] Chotard-Ghodsnia, R., O. Haddad, A. Leyrat, A. Drochon, C. Verdier and A. Duperray. Morphological analysis of tumor cell/endothelial cell interactions under shear flow. *J. Biomech.* 40:335–344, 2007.

[11] Coughlin, M. F., and G. W. Schmid-Schönbein. Pseudopod projection and cell spreading of passive leukocytes in response to fluid shear stress. *Biophys. J.* 87:2035–2042, 2004.

[12] Dalous, J., E. Burghardt, A. Müller-Taubenberger, F. Bruckert, G. Gerisch and T. Bretschneider. Reversal of cell polarity and actin-myosin cytoskeleton reorganization under mechanical and chemical stimulation. *Biophys. J.* 94:1063-1074, 2008.

[13] De, R., A. Zemel and S. A. Safran. Dynamics of cell orientation. *Nature Physics* 3 :655–659, 2007.

[14] Decave, E., D. Garrivier, Y. Bréchet, B. Fourcade and F. Bruckert. Shear flow-induced detachment kinetics of dictyostellium discoideum cells from solid substrate. *Biophys. J.* 82:2383–2395, 2002.

[15] Discher, D.E., P. Janmey and Y. Wang. Tissue cells feel and respond to the stiffness of their

substrate. *Science* : 310:1139–1143, 2005.

[16] Dong, C., X. X. Lei. Biomechanics of cell rolling: shear flow, cell-surface adhesion, and cell deformability. *J. Biomech.* 33:35–43, 2000.

[17] Duffy, D. C., J. Cooper McDonald, O. J. A. Schueller and G. M. Whitesides. Rapid prototyping of microfluidic systems in poly(dimethylsiloxane). *Anal. Chem.* 70:4974–4984, 1998.

[18] du Roure, O., A. Saez, A. Buguin, R. H. Austin, P. Chavrier, P. Silberzan and B. Ladoux. Force mapping in epithelial cell migration. *Proc. Natl. Acad. Sci. USA* 102:2390–2395, 2005.

[19] Gaver, D. P. and S. M. Kute. A theoretical model study of the influence of fluid stresses on a cell adhering to a microchannel wall. *Biophys. J.* 75:721–733, 1998.

[20] Gutierrez, E. and A. Groisman Quantitative measurements of the strength of adhesion of human neutrophils to a substratum in a microfluidic device. *Anal. Chem.* 79:2249–2258, 2007.

[21] Hammer, D.A. and D. A. Lauffenburger. A dynamical model for receptor-mediated cell adhesion to surfaces. *Biophys. J.* 52:475-487, 1987.

[22] House, S. D., H. H. Lipowsky. In vivo determination of the force of leukocyte-endothelium adhesion in the mesenteric microvasculature of the cat. *Circ. Res.* 63:658–668, 1998.

[23] Irima, D., G. Charras, N. Agrawal, T. Mitchison and M. Toner. Polar stimulation and constrained cell migration in microfluidic channels. *Lab Chip* 7:1783–1790, 2007.

[24] Kwon, K. W., S. S. Choi, S. H. Lee, B. Kim, S. N. Lee, M. C. Park, P. Kim, S. Y. Hwang and K. Y. Suh Label-free, microfluidic separation and enrichment of human breast cancer cells by adhesion difference. *Lab Chip* 7:1461–1468, 2007.

[25] Lawrence, M.B. and T. A. Springer. Leukocytes roll on a selectin at physiological flow rates: Distinction from and Prerequisite for Adhesion through lntegrins. *Cell* 65:859–873, 1991.

[26] Li, B., L. Xie, Z. C. Starr, Z. Yang, J. L. Lin and J. H. C. Wang. Development of micropost force sensor array with culture experiments for determination of cell traction forces. *Cell Motil. Cytoskeleton* 22:509–518, 2007.

[27] Lo, C. M., H. B. Wang, H.B., M. Dembo and Y. L. Wang. Cell movement is guided by the rigidity of the substrate. *Biophys. J.* 79:144–152, 2000.

[28] Lu, H., L. Y. Koo, W. M. Wang, D.A. Lauffenburger, L. G. Griffith and K. F. Jensen. Microfluidic shear device for quantitative analysis of cell adhesion. *Anal. Chem.* 76:5257–5264, 2004.

[29] Makino, A., M. Glogauer, G. M. Bokoch, S. Chien and G. W. Schmid-Schönbein. Control of

neutrophil pseudopods by fluid shear: role of Rho family GTPases. *Am. J. Physiol.* 863:C871–C1674, 2005.

[30] Miles, F. L., F. L. Pruitt, K. L. van Golen and C. R. Cooper. Stepping out of the flow: capillary extravasation in cancer metastasis. *Clin. Exp. Metastasis* online first, 2007.

[31] Moazzam, F., F. A. DeLano, B. Zweifach and G. W. Schmid-Schönbein. The leukocyte response to fluid stress. *Proc. Natl. Acad. Sci. USA* 94:5338–5343, 1997.

[32] Munevar, S., Y-L. Wang and M. Dembo. Distinct roles of frontal and rear cell-substrate adhesions in fibroblast migration. *Mol. Biol. Cell* 12:3947–3954, 2001.

[33] Okada, T., H. Okuno, H. Mitsui. A novel in vitro assay system for transendothelial tumor cell invasion: significance of E-selectin and alpha 3 integrin in the transendothelial invasion by HT1080 fibrosarcoma cells. *Clin. Exp. Metastasis* 12:305–314, 1994.

[34] Paul, R., P. Heil, J. P. Spatz and U. S. Schwartz. Propagation of mechanical stress through the actin cytoskeleton toward focal adhesions: model and experiment. *Biophys. J.* 94:1470–1482, 2008.

[35] Pierres, A., A. M. Benoliel and P. Bongrand. Measuring the lifetime of bonds made between surface-linked molecules. *J. Biol. Chem.* 270:26586–26592, 1995.

[36] Pozrikidis, C. Shear flow over a protuberance on a plane wall. *J. Eng. Math.* 31:29–42, 1997.

[37] Reinhart-King, C. A., M. Dembo and D. H. Hammer. The dynamics and mechanics of endothelial cell spreading. *Biophys. J.* 89:676–689, 2005.

[38] Riveline, D., E. Zamir, N. Q. Balaban, U. S. Schwarz, T. Ishizaki, S. Narumiya, Z. Kam, B. Geiger and A. D. Bershadsky. Focal contacts as mechanosensors: externally applied local mechanical force induces growth of focal contacts by an mDia1-dependent and ROCK-independent mechanism. *J. Cell. Biol.* 153:1175-1186, 2001.

[39] Saadi, W., S-J. Wang, F. Lin and N. L. Jeon. A parallel-gradient microfluidic chamber for quantitative analysis of breast cancer cell chemotaxis. *Biomed. Microdev.* 8:109–118, 2006.

[40] Springer T. A. Traffic signals for lymphocyte recirculation and leukocyte emigration: the multistep paradigm. *Cell* 76: 301–314, 1994.

[41] Théry, M. V. Racine, M. Piel, A. Pépin, A. Dimitrov, Y. Chen, J. Sibarita and M. Bornens. Anisotropy of cell adhesive microenvironment governs cell internal organization and orientation of polarity. *Proc. Natl. Acad. Sci. USA* 103:19771-19776, 2006.

[42] Thoumine, O., T. Ziegler, P. R. Girard and R. M. Nerem. Elongation of confluent endothelial

cells in culture: the importance of fields of force in the associated alterations of their cytoskeletal structure. *Exp. Cell Research* 219:427–441, 1995.

[43] Verdier, C. Review. Rheological properties of living materials: From cells to tissues J. Theor. Med. 5:67–91, 2003.

[44] Verdier, C., C. Couzon, A. Duperray and P. Singh. Modelling cell interactions under flow. *J. Math. Biol.* in press, doi 10.1007/s00285-008-0164-4, 2008.

[45] Wankhede, S. P., Z. Du, J. M. Berg, M. W. Vaughn, T. Dallas, K. H. Cheng and L. Gollahon. Cell detachment model for an antibody-based microfluidic cencer screening system. *Biotechnol. Prog.* 22:1426–1433, 2006.

[46] White, F. M. Fluid mechanics. New York : McGraw-Hill, 2003.

[47] Young, E. W. K., A. R. Wheeler and C. A. Simmons. Matrix-dependant adhesion of vascular endothelial cells in microfluidic channels. *Lab Chip* 7:1759–1766, 2007.

FIGURE CAPTIONS

Figure 1: Full view of the experimental set-up. The microfluidic device is placed in a thermostated chamber at 37° C under the x20 objective of an up-right phase contrast microscope. Fluid flow is controlled by a seringe-pump. Before reaching the microchannel, the fluid first passes through the bubble trap (completely filled with medium before the experiment), where bubbles remain trapped.

Figure 2: Schematic view of the microchannel (height h, width w and length L) used in the experiments, with a cell (nucleus N) adhering to the bottom wall. The system of coordinates chosen to describe the flow field ($-w/2 < x < w/2$, $0 < y < h$ and $0 < z < L$) and the velocity profile in a cell free channel are represented on the left.

Figure 3: $\sigma_{zy}(x, 0, z)$ (WSS) at the bottom of a parallelepipedic channel ($w = 1\ mm$, $h = 200\ \mu m$, $Q = 2.10^{-8}\ m^3.s^{-1}$). The WSS is almost constant accross the x axis, except in the regions close to the vertical walls.

Figure 4: Contour of T24 cell drawn with a graphic pad and measurement of cell parameters (area, perimeter, ellipse axes and angle, circularity index defined as $\frac{4\pi\ area}{perimeter^2}$). The nucleus of the cell is surrounded by the lamellipodium. White arrow shows the flow direction. The black scale represents 10 μm. Channel dimensions: $h = 82\ \mu m$, $w = 1\ mm$, WSS $= 0.26\ Pa$.

Figure 5: a) Area versus time $A(t)$ for a T24 cell adhering to the bottom wall of a microchannel ($w = 1\ mm$, $h = 61\ \mu m$) and submitted to a flow increasing every 5 minutes. The black dots represent measurements using the ImageJ software (NIH Image, Bethesda, USA) and the thin dashed line is the polynomial fit. Wall shear stress values are given on the top axis. b) Corresponding area change $\frac{dA}{dt}$ versus WSS. The black dots represent the mean slope of $A(t)$ for a shear stress value and the thick dashed line guides the eye.

Figure 6: T24 area in static conditions: a) Initial spreading is fast until reaching a plateau, then the area decreases just before cell division (time has been rescaled to $t = 0$ corresponding to the beginning of spreading). b) and c) Areas of the two daughter cells after the cell in graph a) has divided. The dashed lines guide the eye.

Figure 7: Repartition of daughter cells' area in static conditions one hour after cell division.

Figure 8: Phase contrast images of a T24 cell adherent to the bottom of a microchannel ($w = 1\ mm$, $h = 64\ \mu m$) submitted to an increasing shear flow. The white arrow shows the flow direction. The black scale represents 10 μm. a) WSS = 0.64 Pa, b) WSS = 6.36 Pa, c) WSS = 19.1 Pa, d) WSS = 31.7 Pa, e) WSS = 50.8 Pa.

Figure 9: Area evolution for five cells submitted to an increasing flow rate in a microchannel ($w = 1\ mm$, $h = 61\ \mu m$). Corresponding WSS are given on the top axis. Symbols represent experimental data (measured from phase-contrast images of the cells), which have been fitted by a standard polynomial fit (lines). For each fit, the star indicates the maximum area.

Figure 10: Area change versus WSS for five cells submitted to an increasing flow rate in a microchannel ($w = 1\ mm$, $h = 61\ \mu m$). Arrows correspond to the location of the cell maximum.

Figure 11: WSS_c vs. channel height h (at constant $w = 1\ mm$). Data are the mean of the WSS_c measured for all the cells tested in the experiments (10, 5 and 6 cells for the channels heights 68, 155 and 264 μm respectively). The dashed lines are the fit of the results based on the model presented in the discussion: experimental values (black dots) are fitted with the hypothesis of equilibrium between adhesion and hydrodynamic forces: $F_{flow} = F_{ad_z}$. Results of the fit give : $N f_{adh} = 18\ nN$

Figure 12: Schematic views of a cell adhering to a flat surface submitted to a shear flow (flow is from left to right). a) Side view: the cell is modeled as a half-shere (radius R), with a circular lamellipodium (radius R_t). An adhesive force $\overrightarrow{f_{ad_z}}$ (z–component) is applied at each of the N focal adhesion sites. b) Bottom view: dots represent randomly distributed focal adhesion sites, where the individual forces $\overrightarrow{f_{ad_z}}$ are exerced.

Figure 13: WSS_c versus h calculated with the equation (9) for differents values of the Nf_{ad_z} parameter : circles $Nf_{ad_z} = 10\,nN$, squares $Nf_{ad_z} = 30\,nN$, triangles $Nf_{ad_z} = 50\,nN$. In three cases, $R = 18\ \mu m$.

Figure 14: Images of an adhering cell after application of successive stresses until the plateau is reached, i.e. the cell maintains a constant area : Phase contrast image, (indirect) immunofluorescence image of the paxillin molecules, corresponding focal adhesion zones obtained after image processing (maximum intensity levels only). The total number of adhesion zones is 31 and their average size is $2.5\,\mu m^2$, corresponding to a total adhesion area (sum) of $78\,\mu m^2$. The total cell area is $2140\,\mu m^2$. The white scale bar represents $10\mu m$.

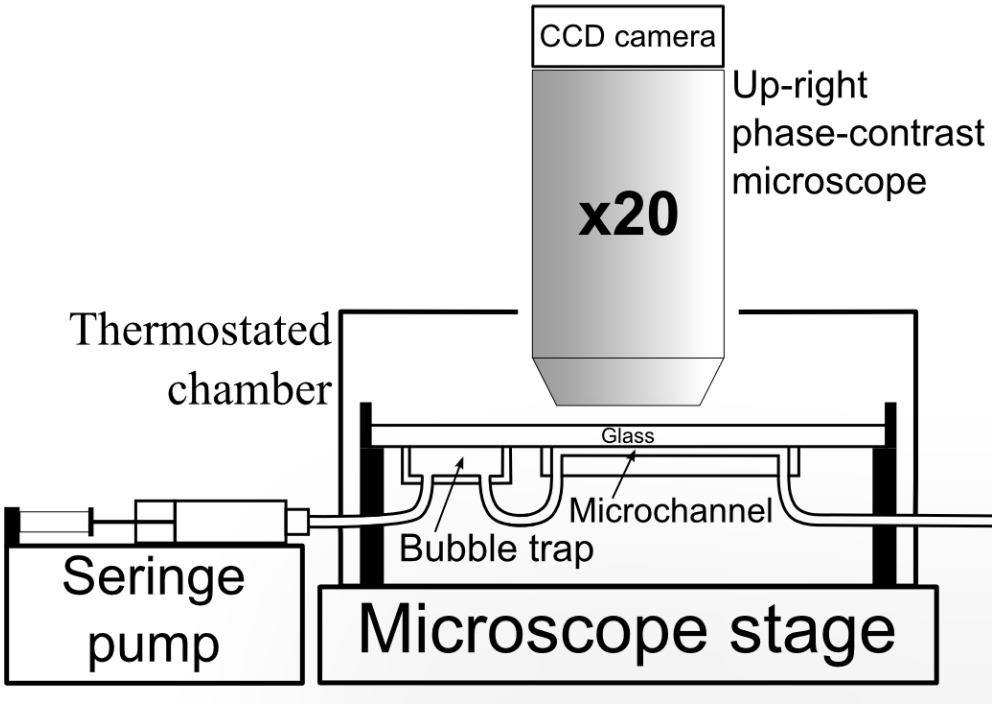
CCD camera
Up-right
phase-contrast
microscope
x20
Thermostated
chamber
Glass
Microchannel
Bubble trap
Seringe
pump
Microscope stage

FIG. 1:

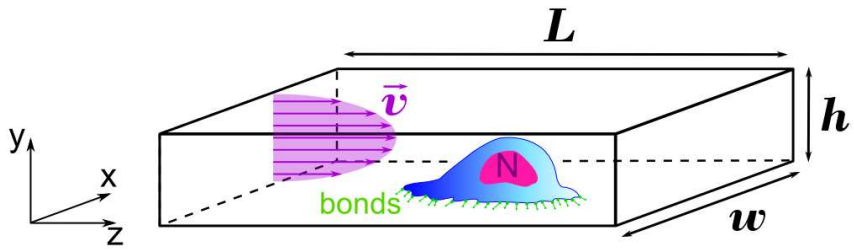

FIG. 2:

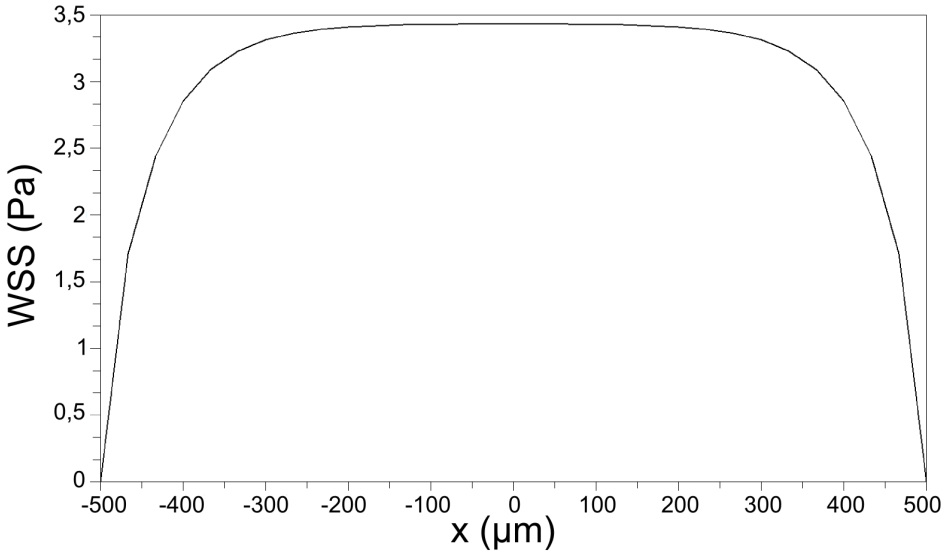
3,5
3
2,5
2
1,5
1
0,5
0
WSS (Pa)
-500
-400
-300
-200
-100
0
100
200
300
400
500
x (µm)

FIG. 3:

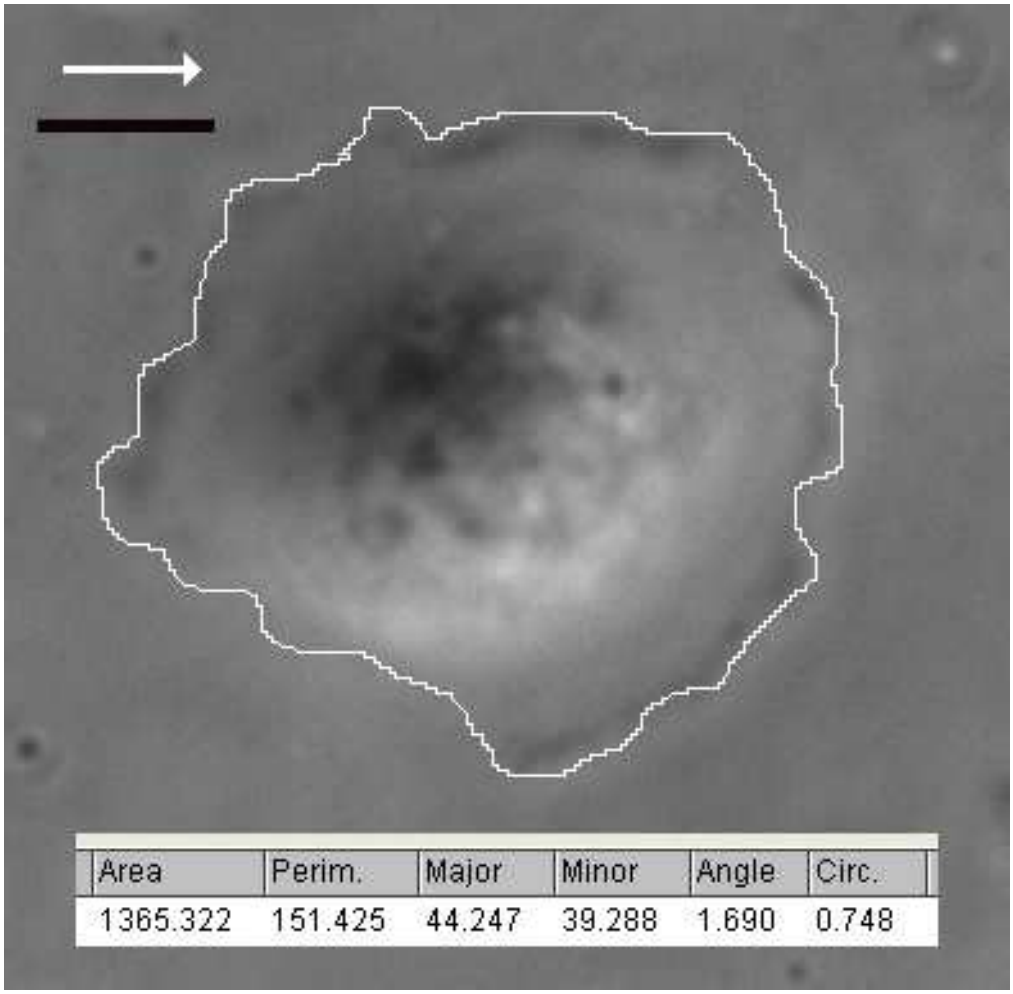
Area
Perim.
Major
Minor
Angle
Circ.
1365.322
151.425
44.247
39.288
1.690
0.748

FIG. 4:

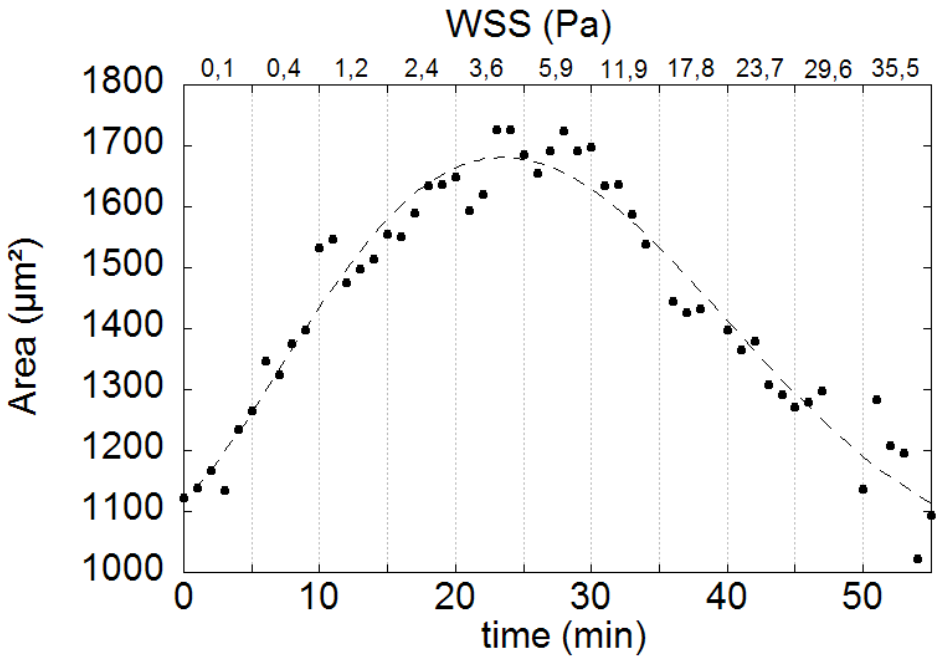
WSS (Pa)
0,1
0,4
1,2
2,4
3,6
5,9
11,9
17,8
23,7
29,6
35,5
Area (µm²)
1800
1700
1600
1500
1400
1300
1200
1100
1000
0
10
20
30
40
50
time (min)

FIG. 5:

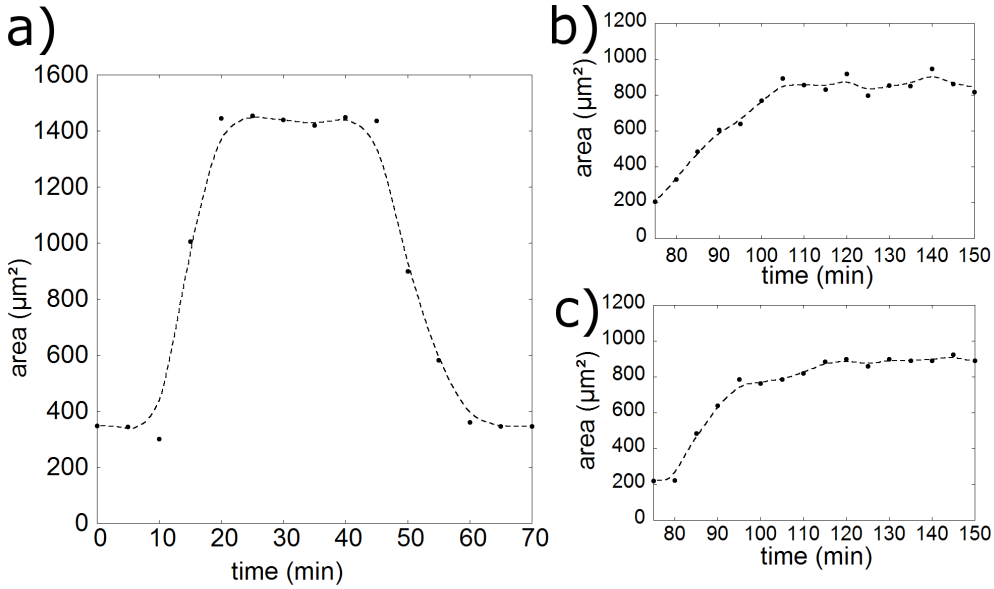

FIG. 6:

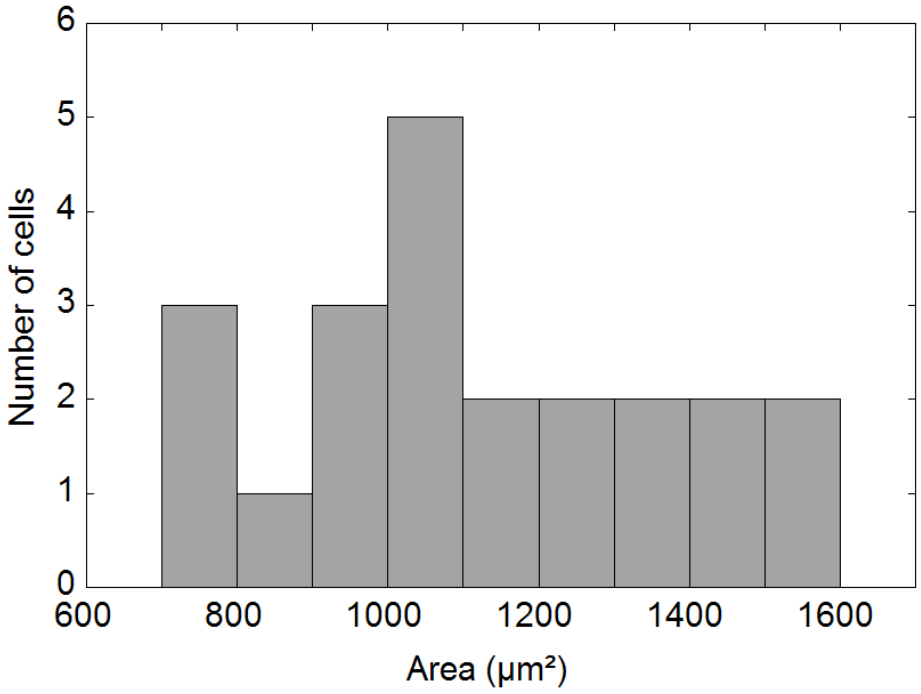

FIG. 7:

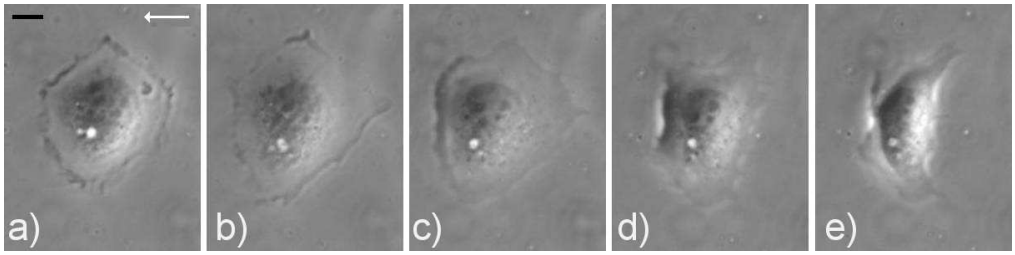

FIG. 8:

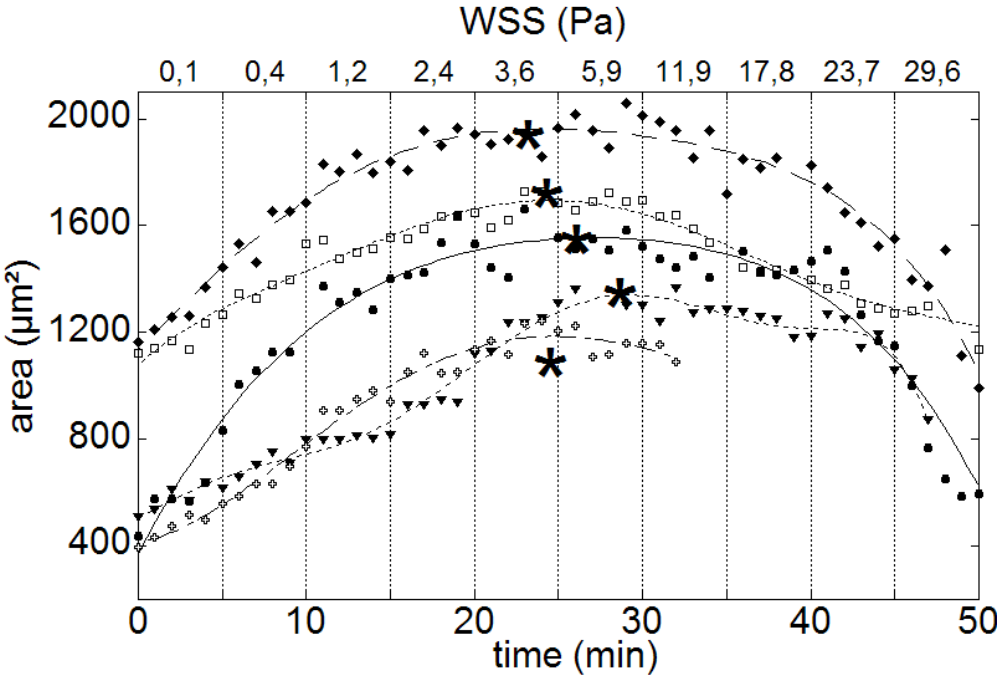
WSS (Pa)
0,1
0,4
1,2
2,4
3,6
5,9
11,9
17,8
23,7
29,6
2000
1600
1200
800
400
area (µm²)
0
10
20
30
40
50
time (min)

FIG. 9:

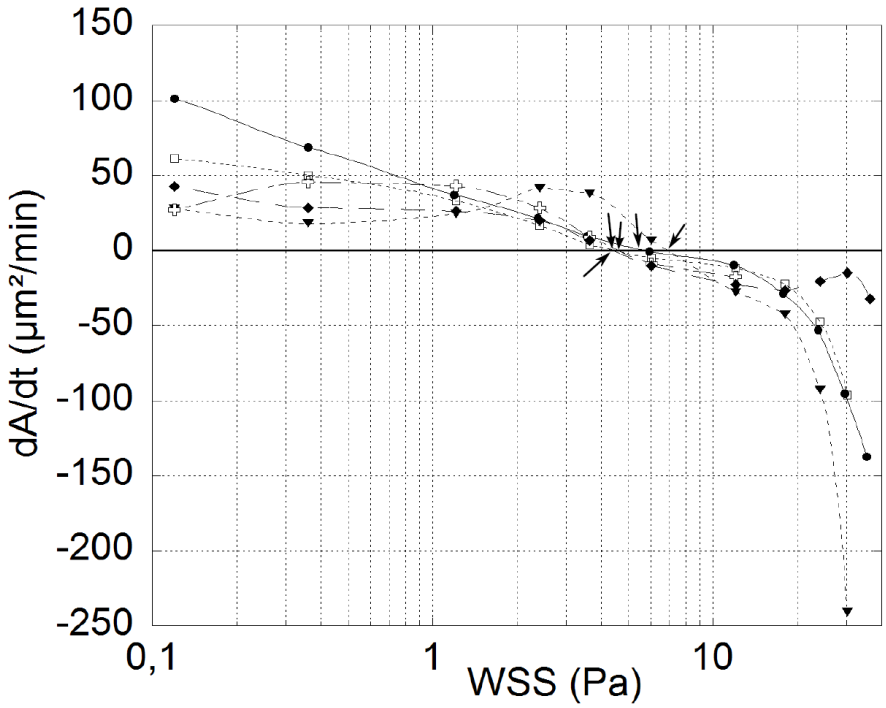

FIG. 10:

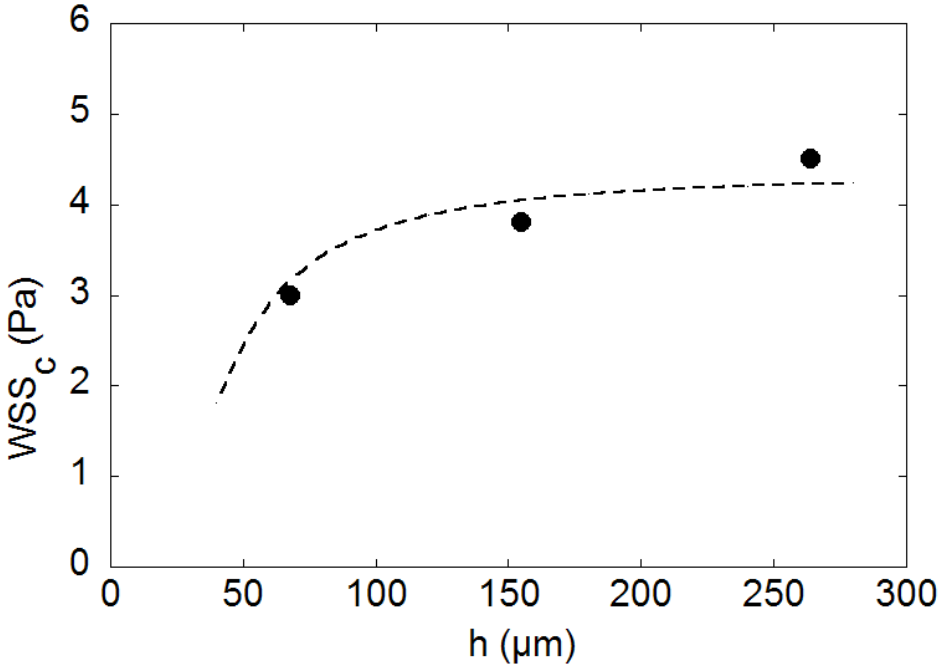

FIG. 11:

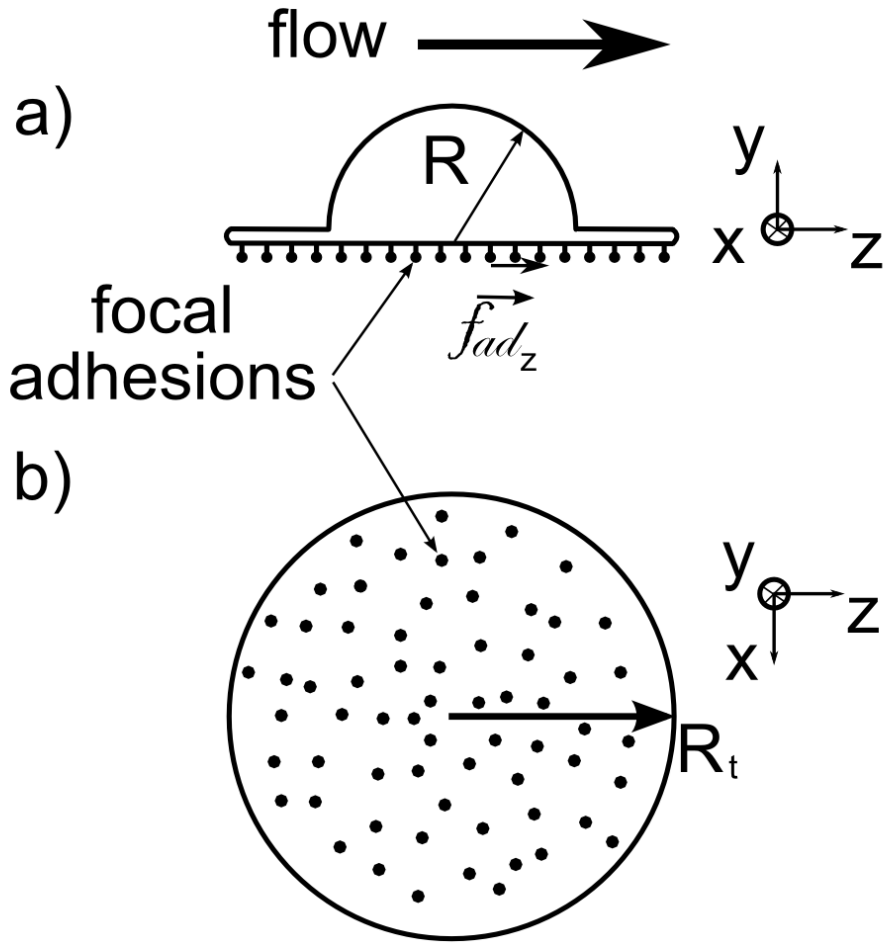

FIG. 12:

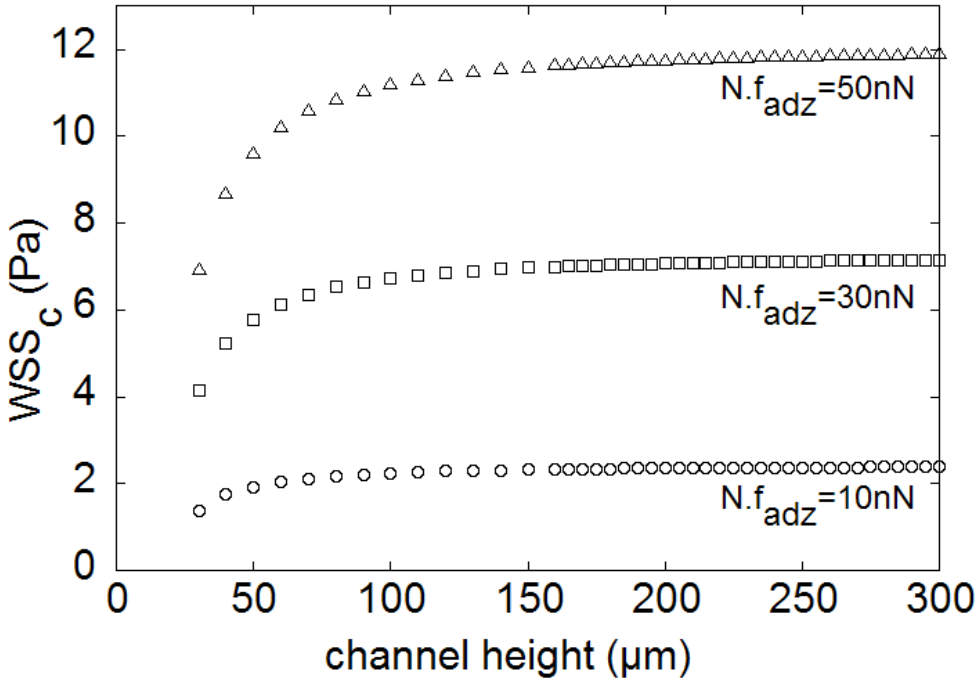
12
10
8
6
4
2
0
WSS$_c$ (Pa)
0
50
100
150
200
250
300
channel height (μm)
N.f$_{adz}$=50nN
N.f$_{adz}$=30nN
N.f$_{adz}$=10nN

FIG. 13:

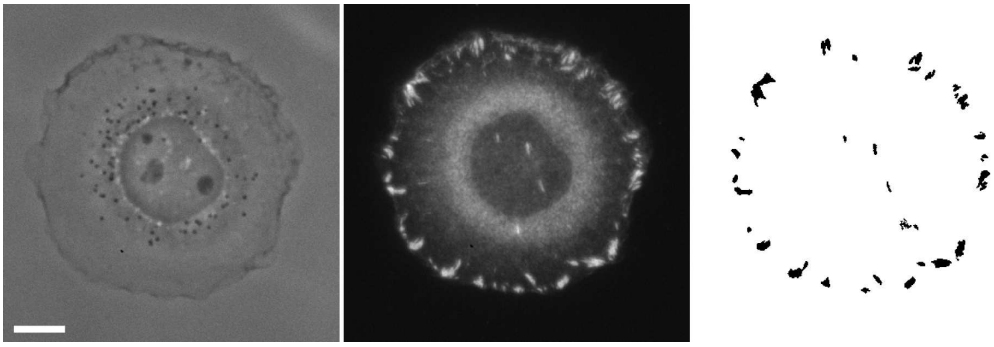

FIG. 14: